Forces in Mechanics 10 (2023) 100163

Contents lists available at ScienceDirect

Forces in Mechanics

journal homepage: www.sciencedirect.com/journal/forces-in-mechanics

Muscle activity on head-first compression responses of a finite element neck model

Mohammad Nasim *, Ugo Galvanetto

Department Industrial Engineering, Industrial Engineering, University of Padova, Padova, PD 35133, Italy

ARTICLE INFO

Keywords:
Finite element model
Muscle modeling
Active muscle
Neck injury
Compressive impact

ABSTRACT

Effects of muscle activation on human neck kinematic responses under compressive loads have not been understood empirically due to the limitation of testing on in vivo test specimens. Advanced computational models can potentially provide information to improve our understanding of such responses. This study used a previously developed ligamentous finite element (FE) neck model, further integrated with muscles, fleshy tissue, and skin of the neck to predict the influence of passive and active muscles on responses to neck compression. For validation, post-mortem human subject (PMHS) and volunteer responses in frontal sled impacts were used to compare the dynamic response of the model with passive and active muscles, respectively. An objective evaluation of the validation responses suggested the 'fair' to 'good' biofidelity rating of the muscular system model. The compressive impacts, used to validate the ligamentous FE neck, were methodologically applied in the current study including the muscles with various activation states, flesh, and skin. The contribution of muscles (passive or active) resulted in an increase in the peak lower neck compression and shear forces and in a reduction in the upper neck forces on average; the role of active state dynamics of the muscles was crucial on the magnitude of the forces. Therefore, modeling of the muscles in a computational neck model may not be neglected to study a head-first compressive impact.

1. Introduction

Despite cervical spine compression is one of the main causes of serious neck injuries in motor vehicle accidents [1,2], little advanced research has been carried out to better understand the complex dynamic behavior of a humanlike neck in compression to predict injuries. Empirical impact data explaining compressive behavior of a neck with active or passive muscles are not available, to our knowledge, presumably due to difficulties in handling and testing physical subjects. Compressive impact tests with volunteers are not favorable due to the associated risk of injuries. The PMHS experiments are expensive and complex. Furthermore, PMHS lacks muscle activation. Therefore, advanced computational models can significantly improve understanding of the effects of muscles on the kinematic response of a humanlike neck.

In this paper, we use a previously developed ligamentous FE neck model (D-neck), which was validated under head-first compressive loadings at the global level and with bending moments at the segment level [3]. As a further advance of the model, this paper describes the generation of muscles, neck skin, and soft fleshy tissue and validates the model for muscles. The D-neck, as a computationally efficient tool for large and systematic parametric studies, was developed to assess motorcycle neck protective equipment based on injury risk prediction at the global level, particularly during head-first compression. However, the absence of muscle activity was a limitation for accurate results.

Based on the mechanical behavior of the muscles, it can be hypothesized that the muscle modeling is important in tension-based inertial loading and may be neglected for the neck response in compression. Verification of the hypothesis is needed to understand the importance of complex modeling of the neck musculature for studies with compressive loading, which may possibly lead to numerical instabilities. Although several computational neck models have been developed with muscle activation [4–12], we noticed that only Nightingale et al. (2016) investigated the hypothesis underlined and concluded that active muscles affect the neck response with larger compressive and shear forces [13]. However, the results were essentially based on a computational study with an optimized muscle activation scheme in a specific neck model. The passive and active model responses

* Corresponding author.
E-mail address: mns_10@hotmail.com (M. Nasim).

https://doi.org/10.1016/j.finmec.2022.100163
Received 4 November 2022; Received in revised form 16 December 2022; Accepted 25 December 2022
Available online 26 December 2022

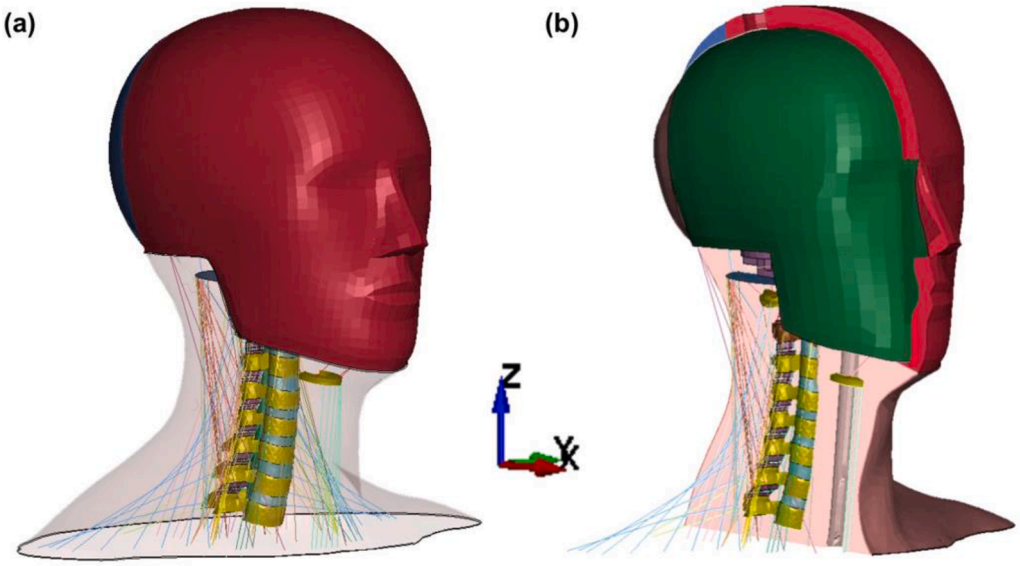

Fig. 1. Latero-anterior views of (a) the position of muscles in the neck model and (b) the entire musculature neck model including the neck skin and flesh (shown as section views in the sagittal plane).

under compression were not compared. What is not yet clear is which activation states govern muscles during realistic head-first compressive impacts and how they influence the neck response. Therefore, the objective of this study is to further investigate the muscle activity under compression for various levels of muscle activation (zero activation for passive muscles) using a different neck model. The results should provide a better understanding of the influence of muscles on neck impact responses during head-first compression.

2. Methods

The head-neck assembly was constructed using the hybrid III head model (50th percentile male), developed by LSTC (Livermore Software Technology Corporation), and the previously validated ligamentous D-neck model [3]. All normally terminated simulations of this study were solved using the explicit LS-Solver (version R810, double precision executable) on Intel Xeon CPU E3-1270 v5 3.6 GHz processors. The global coordinate system was considered with the X-axis (forward), Y-axis (left), and Z-axis (upward). Force data and moment data were filtered at 1000 Hz and 600 Hz, respectively, following the SAE J211 specifications.

2.1. D-neck model

The segmented neck (C0-T1) of the D-neck model consists of 94,997 elements, which includes vertebrae, intervertebral discs (annulus fibrosus and ground substances), ligaments, spinal cord, and facet cartilages. The compatibility assessment by Nasim et al. (2021) suggested that the model is comparable to a 50th percentile human neck [3]. In this paper, the muscles, along with the soft fleshy tissue and the skin of the neck, were integrated into the model. Fig. 1 illustrates the musculature neck model, including the flesh and the skin.

2.1.1. Muscles

The modeled muscles used a total of 186 1D Hill-type beam elements. The origin and insertion nodes of the muscle elements were determined with the aid of the clinical anatomy literature [7,14–16], where the vertebrae, the skull, and the base of the fleshy part of the model were taken as references. A total of 93 pairs of symmetric muscle were used to model 25 different muscle groups of the neck (see Table A1 in Appendix for the list of the muscle groups and the physical muscle properties). A simple hyoid bone was generated and positioned at the level of C3 (can be seen in Fig. 1) for correct insertion of the infrahyoid and suprahyoid muscles and was modeled with the constitutive material behavior identical to cortical bones.

Each muscle length was calculated as the average distance from the origin to the insertion nodes. Data of physiological cross-sectional area (PCSA) and muscle volume were taken from the information provided by Borst et al. (2011) [16], except for the suprahyoid muscle, which was taken from Pearson et al. (2011) [17]. The PCSA was equally divided to each segment of a specific muscle and the weight was distributed according to the average length of a muscle group generated in the model.

The Hill muscle model incorporates a contractile element and a passive element [18]. The force generated in each muscle is the total of the force contribution by the contractile and passive elements. The active muscle force, generated by the contractile element during muscle activation, is a function of the activation level, velocity, and length of the muscle, as given in Eq. (1) [19].

$$F_{contractile} = F_{max} \,.\, a(t) \,.\, F_v(v) \,.\, F_l(l) \tag{1}$$

The maximum isometric force (F_{max}) was calculated as the product of physiological cross-sectional area (PCSA) and maximum muscle stress (σ_{max}). Muscle activation level–time, force-velocity, and force-length relationships, as shown in Table 1, were provided in Hill-type elements to define active muscle properties. The maximum strain rate ($\dot{\varepsilon}_{max}$) for the force-velocity relationship was defined. The muscle activation state, following EMG signals, was adopted from the work of Panzer et al. (2011), in which the active state multiplier curve for the flexor and extensor muscles was considered the same [9].

The force contributed by the passive element is calculated by Eq. (2) [18],

$$F_{passive} = \frac{F_{max}}{e^{C_{PE}} - 1}\left[e^{\left(\frac{C_{PE}}{\varepsilon_{max}}\varepsilon\right)} - 1\right] \tag{2}$$

where ε = strain, C_{PE} = constant for dimensionless stress versus strain function, and ε_{max} = strain when the stress of the passive element reaches its maximum isometric stress value.

2.1.2. Skin and fleshy tissue

The neck skin geometry was adopted from a 50th percentile male avatar provided in the commercial software CLO®. The skin ranged

Table 1
Constitutive behavior and material properties of the modeled tissues.

Tissue	Constitutive law [LS-DYNA mat model]	Material properties	Reference
Muscles	Hill-type muscle [156]	$\sigma_{max} = 0.5$ MPa	[23]
		$a\ (t)$ - 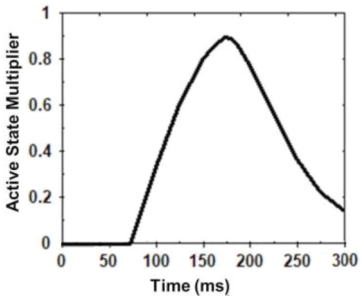	[9,19]
		$F_v\ (v)$ - 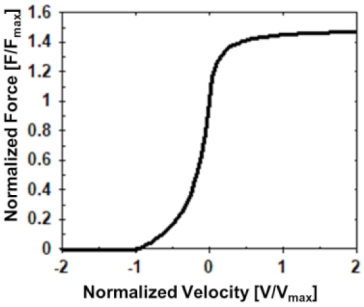	
		$F_l\ (l)$ - 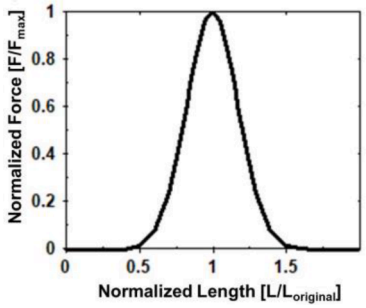	
		$\dot{\varepsilon}_{max} = 8\ (l_{opt})\ s^{-1}$	[24]
		$\varepsilon_{max} = 0.6$	[25]
		$C_{PE} = 3$	[25]
Flesh	Incompressible hyperelastic [077_O]	$G_1 = 3$ kPa, $\beta_1 = 310\ s^{-1}$, $\nu = 0.499$, $\mu_1 = 0.03$ kPa, $\alpha_1 = 20$	[11,22]
Skin	Isotropic elastic [001]	$E = 6$ MPa, $\nu = 0.4$	[11,21]

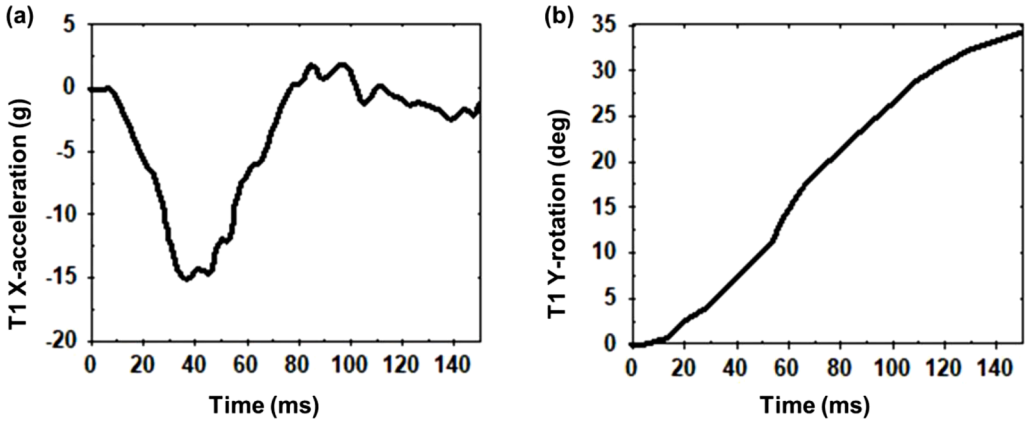

Fig. 2. Average T1 (a) X-acceleration and (b) Y-rotation as input for the simulation of the 18g frontal impact.

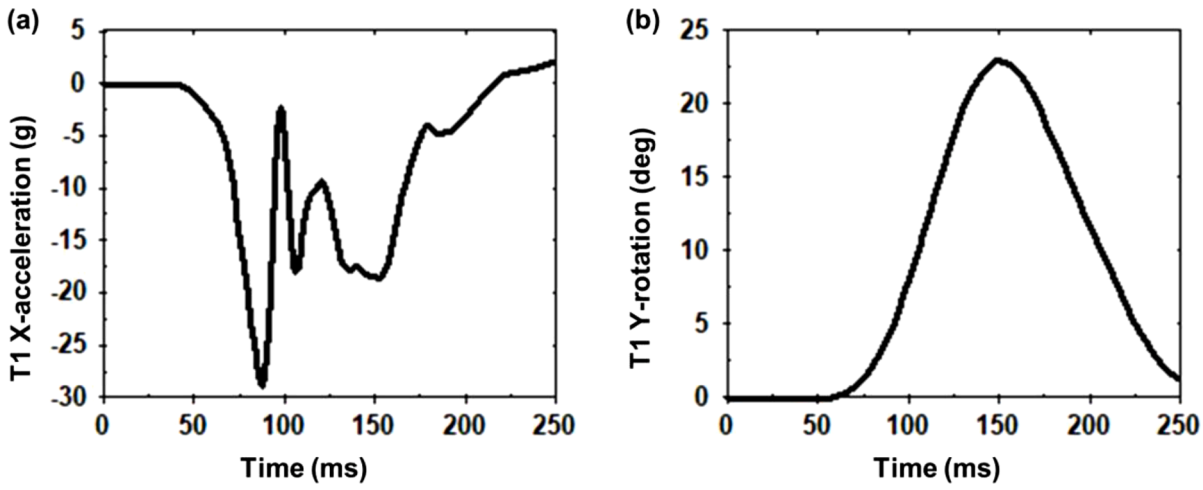

Fig. 3. Average T1 (a) X-acceleration and (b) Y-rotation as input for the simulation of 15g frontal impact.

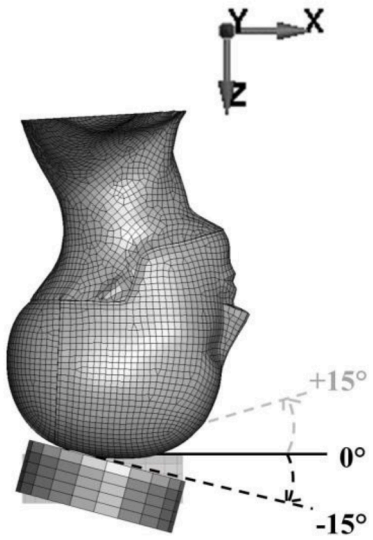

Fig. 4. Head-first compressive impact simulation with the full neck model at the impact angles of - 15°, 0°, and + 15°.

from the inferior part of the hybrid III head to the clavicle at second thoracic vertebra (T2) level, as shown in Fig. 1b. We assumed that the skin was 0.9 mm thick [20]. The modeled skin was generated with 2,942 brick elements and isotropic elastic material model using the linear stress-strain relationship (Eq. (3)) [11,21], where σ is the stress, ε is the strain, E is the Young's modulus.

$$\sigma = E\varepsilon \tag{3}$$

The latest construction of the model includes fleshy soft tissue, generated within the void volume of the skin (Fig. 1b). Contact between the flesh and the segmented cervical spine model was neglected, as the flesh modeling was intended to improve the accuracy of the skin response. A total of 1,90,834 tetrahedron elements and an Ogden-based hyperelastic formulation were used to model the flesh [11,22]. The Ogden strain energy function used the following Eq. (4) [18].

$$W = \sum_{n=1}^{N} \frac{\mu_n}{\alpha_n}\left(\lambda_1^{\alpha_n} + \lambda_2^{\alpha_n} + \lambda_3^{\alpha_n} - 3\right) \tag{4}$$

where μ and α are the empirical parameters and $\lambda_{i=1,2,3}$ is the principal stretch. The nominal stress yielded for one-term strain energy density is

$$S = \frac{2G}{\alpha}\left\{\lambda^{\alpha-1} - \lambda^{-\left(\frac{\alpha}{2}+1\right)}\right\} \tag{5}$$

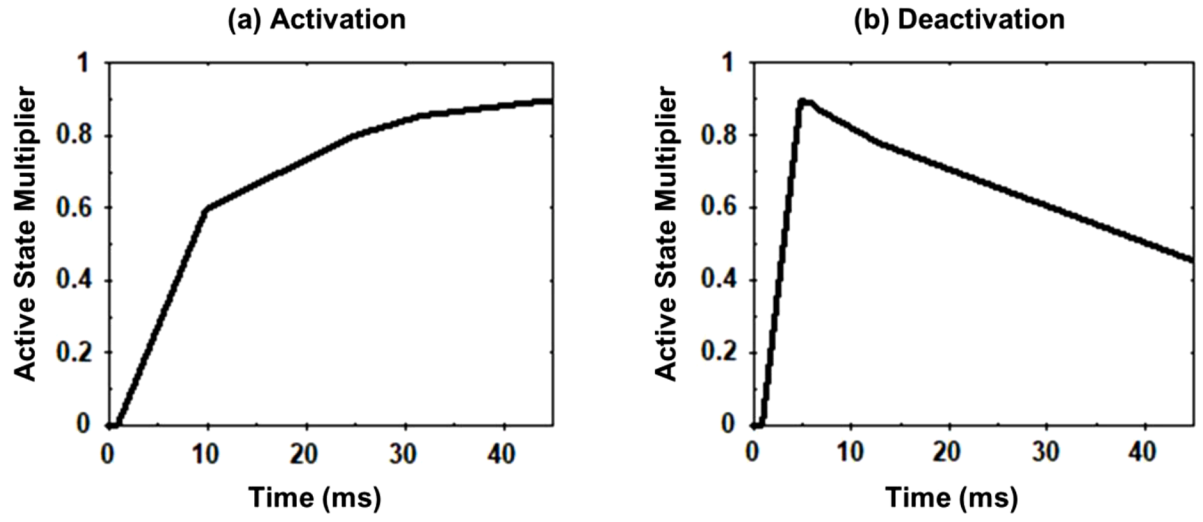

Fig. 5. (a) Activation and (b) deactivation state multipliers for the contractile muscle force in compressive impact simulations.

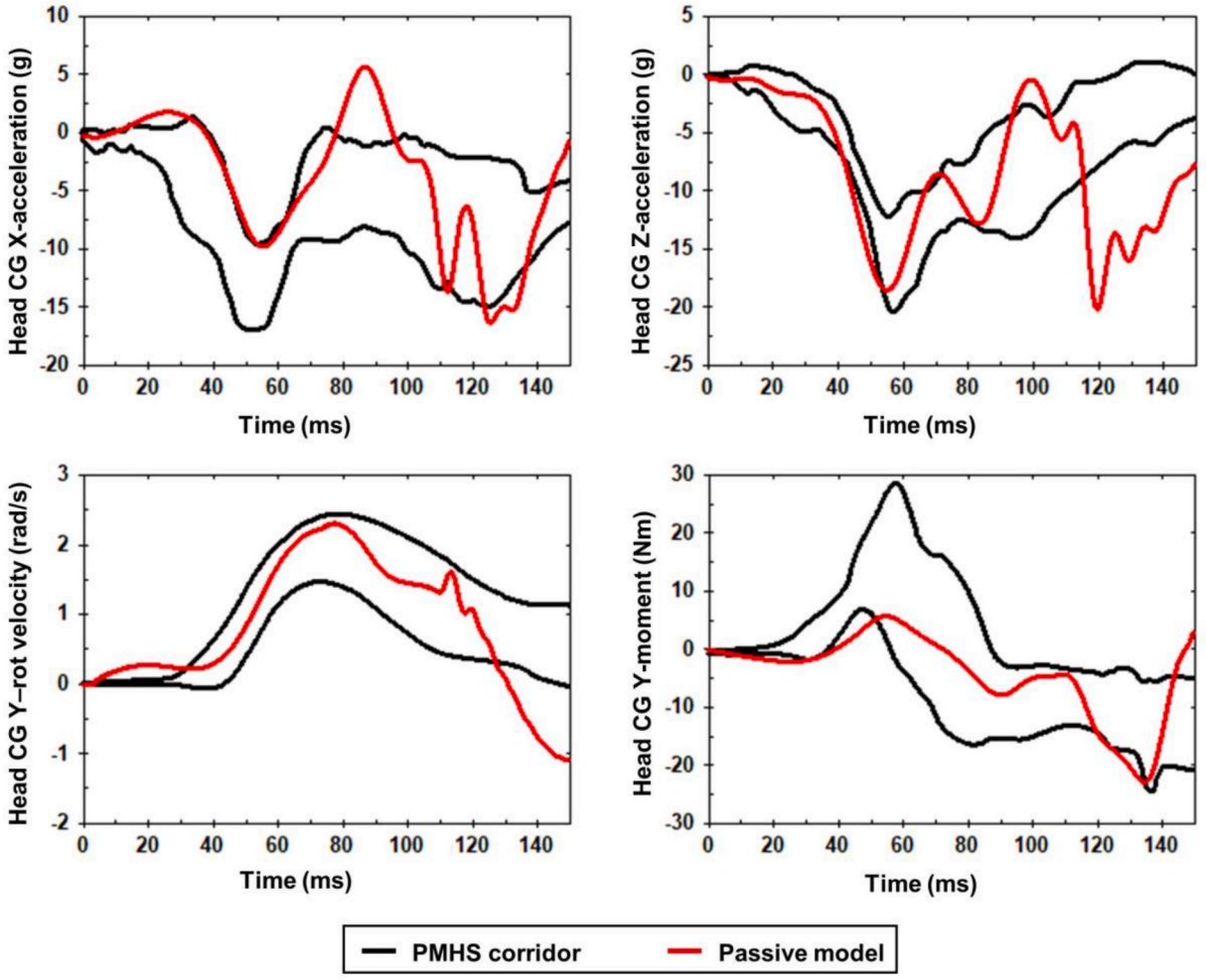

Fig. 6. Results of the 18g frontal impact simulation with passive neck model. The computed head CG X-acceleration, Z-acceleration, Y-rotational velocity, and Y-moment were compared with the experimental corridors (mean ± 1 SD) conducted with the PMHS.

where G (>0) is the shear modulus at infinitesimal strains and λ is the stretch ratio in the compression direction. A shear relaxation function ($g(t)$) was used as

$$g(t) = \sum_{i=1}^{n} G_i e^{-\beta_i t} \tag{6}$$

where β is the decay constant.

The trachea cavity, passing through the hyoid bone, was also introduced into the fleshy part. The material properties used in the governing constitutive behavior of muscles, skin, and flesh are given in Table 1.

2.2. Validation method

The current FE neck model with ligaments was validated dynamically at global level under compression and quasi-statically at segment level under flexion/extension moment in the previous study [3]. The results of the biofidelity assessment showed that the model could exhibit a good biofidelic response. In this paper, the focus was to validate the model response based on muscle activation level. Due to the unavailability of empirical compressive data, different loading conditions were used in the current validation methods, which essentially provided a check of the biofidelity of muscle modeling.

2.2.1. Model with passive muscles under 18g frontal impact

Passive muscle modeling of the FE neck was validated using empirical studies conducted on five unembalmed PMHS under frontal impact [26,27]. The tests conducted at 6.9 m/s velocity (average sled acceleration of 18g) were used for the validation. The average T1 motion (only forward acceleration and sagittal rotation, as shown in Fig. 2) was prescribed as boundary conditions for simulation. It was assumed that the T1 frontal acceleration [28] with a significant amount of T1 rotation [29] is the medium for transferring the sled acceleration to the head during the sled tests. Muscle activation in the simulation was set to zero to account for passive muscle contribution only.

2.2.2. Model with active muscles under 15g frontal impact

Model response with muscle activation under 15g frontal impact loading was evaluated against the data of sled tests performed on young male volunteers [30,31]. Vertical or lateral displacement of the T1 vertebra of the volunteers was sufficiently constrained due to the imposed occupant restraint systems. The average T1 motion (forward acceleration and sagittal rotation, as shown in Fig. 3), calculated from the recorded experimental data [31], was prescribed as boundary conditions for simulation; all other motions of the T1 were constrained. All muscles were activated based on the activation state shown in Table 1, in which the activation start was set at 74 ms and was maintained for 100 ms before the deactivation [9].

2.3. Compression test

The dynamic compressive behavior of the musculature neck model

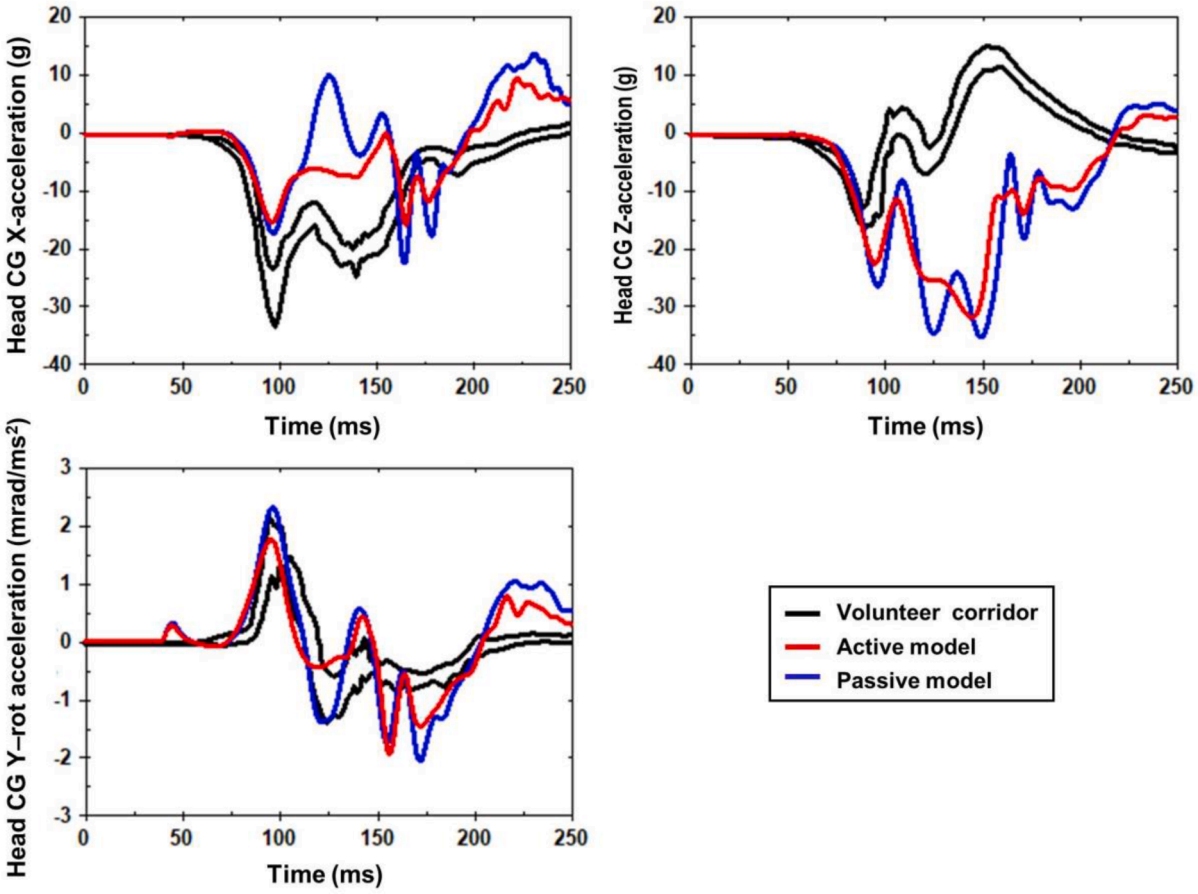

Fig. 7. 15g frontal impact simulation results with both passive and active neck models. The computed head CG X-acceleration, Z-acceleration, Y-rotational acceleration were compared with the experimental corridors (mean ± 1 SD) conducted with volunteers.

during head-first compression was investigated following the inverted drop test method [32–34], as shown in Fig. 4. The boundary conditions applied in the simulations were similar to those used for validation in [3]. The FE head impacted the Teflon layer, placed over the rigid anvil, with an initial velocity of 3.2 m/s in all the simulations. The inferior surface nodes of the modeled skin and flesh were constrained to T1. According to the boundary conditions, the T1 was only allowed to move in the axial direction without any rotational movement. A torso mass of 16 kg was assigned to T1 for experimental homogeneity.

Defining the muscle activation scheme for compression was challenging, as no appropriate neural input signal was found explaining the compressive behavior of the musculature neck. Based on the fact that this current model was developed to assess motorcycle neck protective equipment, the focus was on motorcycle crash scenarios to simulate the impacts. The initial inertial load may result in multiple impacts in motorcycle crashes [35], for which the assumption of an activation state becomes difficult. Therefore, we considered three different muscle state dynamics assuming that head-first compression may occur during any time of muscle activity. First, it was assumed that the muscle did not have time for activation, which was simulated with passive muscles only. Second, it was assumed that the impact occurred when the neural input was activated, as defined by the curve in Fig. 5a. Third, it was assumed that the impact occurred when the neural input was deactivated, as defined by the curve in Fig. 5b. The curves in Fig. 5, defining both the activation and deactivation states of the active muscles, were derived from the muscle activation scheme in Table 1. The simulation environment was set in such a way that the head impacted the anvil at 10 ms; by then, the active muscles reached the required activation or deactivation state.

3. Results

3.1. Response with passive muscles during 18g frontal impact

The dynamic response of the neck model with passive muscles was compared with the PMHS tests for the 18g frontal impact in Fig. 6. The X-acceleration (horizontal), Z-acceleration (vertical), Y-rotational acceleration (sagittal), and Y-moment (sagittal) signals at the CG of the head model were computed and compared with the experimental corridors. The model response showed good agreement with the experimental transient response. However, in some instances, there were small discrepancies between the two responses.

3.2. Response with active muscles during 15g frontal impact

Fig. 7 compares the active musculature model response with the volunteer response for the 15 g frontal impact based on head CG X-acceleration (horizontal), Z-acceleration (vertical), and Y-rotational acceleration (sagittal). Both active and passive muscle responses were compared with experimental corridors to show the need for active muscle modeling to predict the behavior of a real human. Fig. 7 clearly shows that muscle activation is important and may improve the prediction capability of a human subject. Good agreement was observed for the head rotational acceleration in the sagittal plane and the horizontal linear acceleration. The model response showed a poor correlation for the vertical acceleration due to over prediction, which could be marginally accepted.

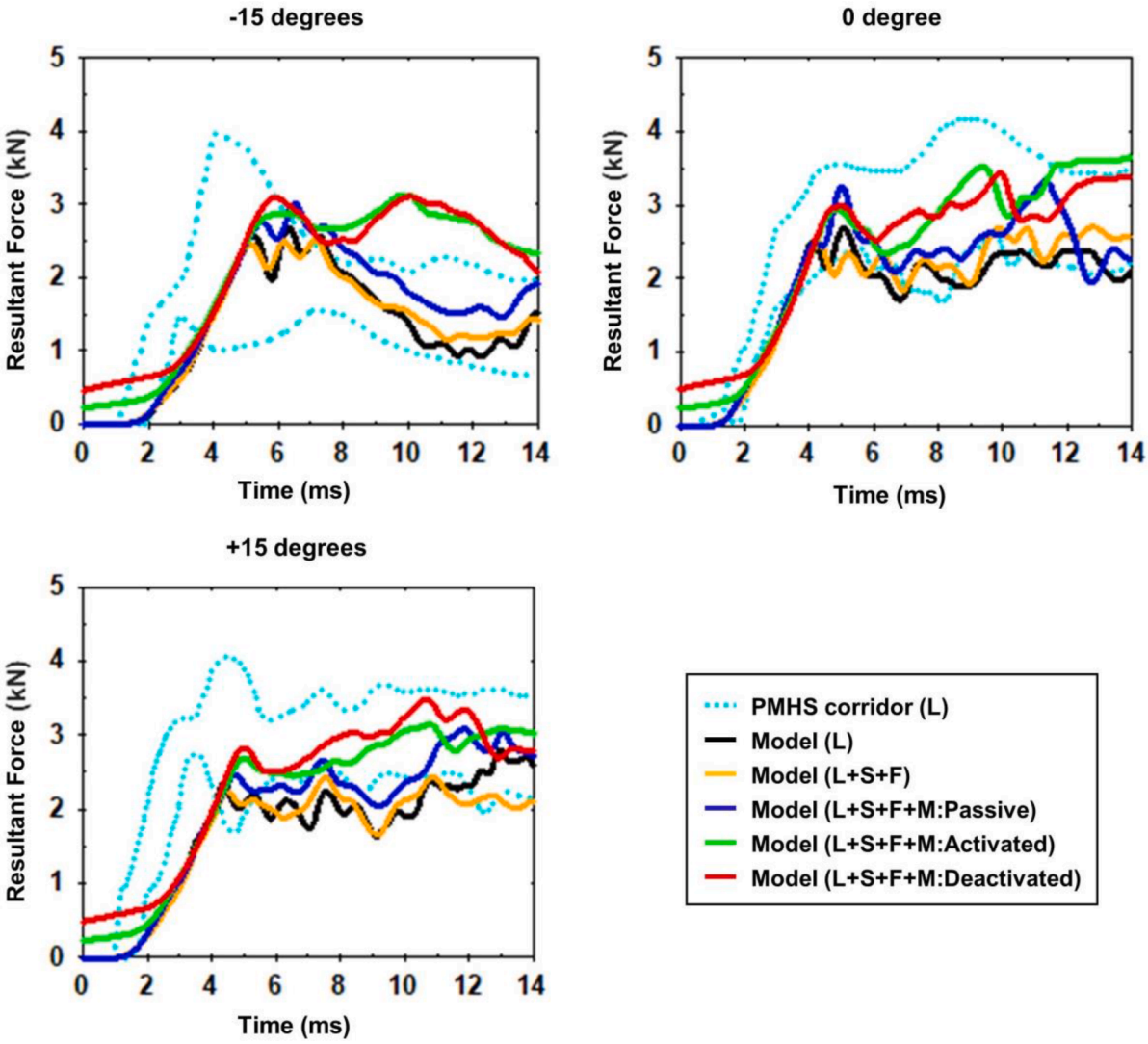

Fig. 8. Resultant neck forces of the model at different component levels compared with PMHS neck response at the impact angles of - 15°, 0°, and + 15°. The letters in the legend indicate the additional component(s) used with the cervical spine of the PMHS and the model: L (ligaments), S (skin), F (flesh), and M (muscle).

3.3. Response of the head-neck complex under compressive impacts

All simulations were analyzed for 15 ms from the time of impact. The time length was sufficient because the injury and the peak axial force were found to occur in less than 10 ms and less than 15 ms, respectively, in the experimental impact tests with PMHS [32,33].

Fig. 8 shows the resultant lower neck forces (measured at T1) of the neck model with ligaments (L), added neck skin and flesh (L+S+F), added passive muscles only (L+S+F+M:Passive), and added active muscles in the activated state (L+S+F+M:Activated) and in the deactivated state (L+S+F+M:Deactivated), compared to the experimental corridors. The corridors were calculated from tests performed on the PMHS ligamentous necks [33–35]. The results show that the peak resultant force increases due to the effects of muscles. The force signals due to active muscles showed different curve patterns, in which the force becomes larger after a few milliseconds of the first peak than in other conditions.

Fig. 9 compares the peak upper and lower neck shear and axial forces calculated at various component levels of the neck model. The upper and lower neck forces were measured at the modeled occipital condyle and T1, respectively. Integration of the neck skin and flesh in the ligamentous neck model affected the neck response by decreasing the shear force and increasing the compressive force in the upper neck. The neck response was further affected when muscles came into play, showing an increase in the peak shear force previously measured with the skin and flesh and a decrease in the peak compressive force. In general, the behavior of the musculature neck suggests that the peak upper neck shear force becomes smaller compared to the ligamentous neck during oblique impacts; however, muscle activation can slightly increase the peak force under pure compression. The peak lower neck shear force normally increases due to the effects of muscles. Muscle integration predictably decreases the peak upper compressive force and increases the peak lower compressive force. Moreover, the activation of the muscles further decreases the compression of the upper neck.

4. Discussion and conclusions

This paper presented the modeling of passive and active muscles and the integration of muscles in a ligamentous FE neck model. The quality of passive and active models was evaluated using experimental data obtained through PMHS and volunteer tests in frontal impacts. The model was then used to investigate the hypothesis of this study that muscle modeling with or without any muscle activation scheme can be neglected to study the compressive response of a neck. This computational study is important as no suitable experimental data were found to support the hypothesis.

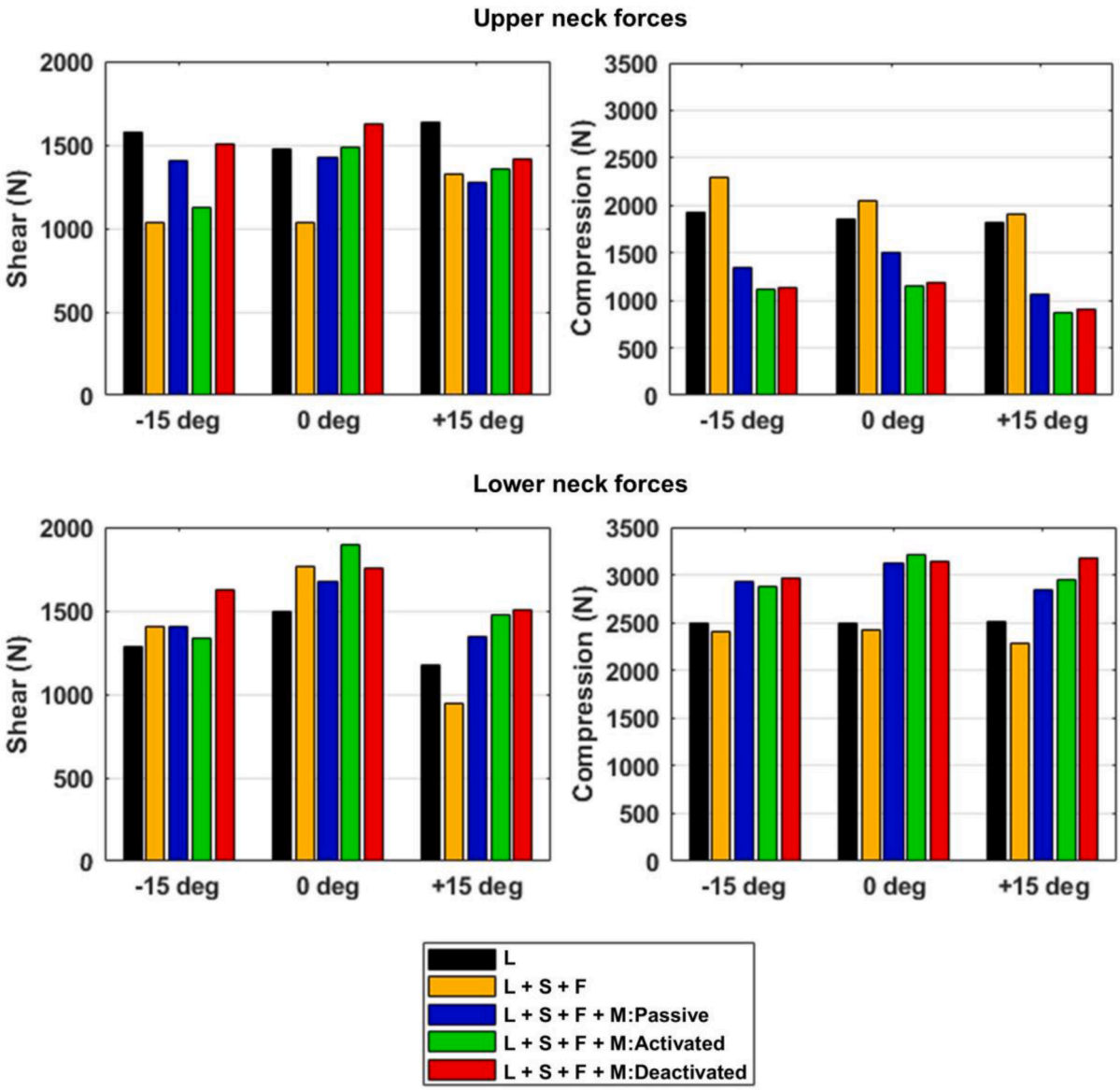

Fig. 9. Peak upper and lower neck shear and axial forces of the neck model at various component levels under compressive impacts. The impact angles were - 15°, 0°, and + 15°. The letters L, S, F, and M in the legend indicate the ligamentous cervical spine, skin, flesh, and muscle, respectively.

The model response was objectively rated using the CORrelation and Analysis (CORA) method [36]; the summary of the rated scores is given in Table A2 (see Appendix). It is a widely accepted standard rating method that provides an objective measure of biofidelity by combining two correlation methods [37]. The first method (corridor) correlates the model response with the experimental corridor, and the second method (cross-correlation) correlates the shape, size, and phase between the simulation and experimental responses. According to the standard, CORA uses a correlation rating score between 0 and 1 that defines the quality of biofidelity [37,38]: excellent ($1 \geq$ score ≥ 0.86), good ($0.86 >$ score ≥ 0.65), fair ($0.65 >$ score ≥ 0.44), marginal ($0.44 >$ score ≥ 0.26), and unacceptable ($0.26 >$ score ≥ 0). For scoring, CORA 3.6.1 software (developed by Partnership for Dummy Technology and Biomechanics) was used. Default parameter values, with the exception of a linear shape function and a linear gradient in the corridor method between one and two standard deviations from the mean experimental data, were used for the CORA in the current study.

The dynamic behavior of the passive musculature model during frontal impact was in good agreement with the PMHS response data and the rated score (0.750) indicated good biofidelity of the model. The volunteer response was also used to compare the passive model response, where the biofidelity score (0.430) became marginal; however, the score (0.547) was improved when the muscles were activated in the model. The kinematic response of the active model exhibited a fair correlation with the volunteer test data. The results clearly explain that muscle activation in the model was reasonable for comparing the neck response with such in vivo test data, as active muscles were present in the volunteers. Several reasons might have affected the quality of the model response and caused divergence in some instances, such as the simplicity of the modeled muscles, the boundary conditions in the simulation, the initial position and neutral curvature of the neck, the accuracy of the muscle activation scheme that was considered common for both extensor and flexor muscles.

Figs. 8 and 9 showed that the inclusion of the flesh and skin without the muscles is insufficient to describe the dynamic response of an advanced neck model. These figures are consistent with previous findings by Nightingale et al. (2016) [13] exhibiting that active muscles play a substantial role in the compression behavior of the lower neck, resulting in larger peak forces at T1. The results contributed additional evidence that passive muscles also increase the peak forces at T1;

however, the forces on average became larger when active muscles came into play. The probable factors contributing to these effects could be the added muscle mass and the generated muscle force. Another possible factor was the applied constraints to torso motion, which was reported to slightly increase the average lower neck compression force [13]. The peak upper neck compression forces at the modeled occipital condyle became smaller because of muscle activity. The mechanical explanation could be that the muscle increased the strength of the neck to resist head motion. Therefore, it is probable that the transmission of force from the head to the upper neck was reduced after the impacts occurred. The reduction in transmitted force became even larger due to the role of active muscles, possibly because of the contractile force generation in the muscles. In addition, the magnitude of the forces showed dependency on the impact angle and on the activation or deactivation state of the muscles.

Several existing limitations to this study should be considered. First, the structural stability of the FE neck was affected presumably due to the simple modeling approach. The previous validation of the model with bending moments at the segment level suggested that the modeled neck is comparatively stiffer than the average PHMS necks. The bending stiffness could have further increased due to the added muscle mass, which provided inertial resistance to buckling [39]. Second, the model response is based on the specific initial neutral curvature of the cervical spine. The effect of pre-bending the cervical spine was not within the scope of this study. Third, simple techniques were applied to model the complex muscle system. The origin or insertion points of several muscles could not be properly defined, as they were constrained to the base of the fleshy part at the T1 vertebra level. Actual neural excitation data to define muscle activation state during head-first compressive impacts was beyond the ability of this study. Moreover, the muscle groups in the model were neither optimized based on the activation level nor preloaded for the equilibrium state. Lastly, the current model may not be applied in specific cases expecting a high degree of confidence from the absolute values of the predicted outputs of this study, as the prediction of the magnitude of the specific mechanical features depends on the input parameters.

Despite its exploratory nature, the present study offers insights into the effects of muscles with or without activation on the dynamic response of the neck during compressive impacts. Finally, our observation suggests that considering muscles to a computational neck model for a head-first compressive impact analysis may not be avoided; however, the muscle activation state should be chosen with caution until further evidence is available to support the validity of the model response.

Declaration of Competing Interest

The authors declare that there is no conflict of interest.

Data Availability

Data will be made available on request.

Acknowledgment

The research leading to these results received funding from the ECCELLENZA programme of the CARIPARO foundation under the REDIPhE project. However, the initial funding support was received from the People Programme (Marie Curie Actions) of the European Union's Seventh Framework Programme FP7/2007-2013/ under REA grant agreement n° 608092.

Appendix

Table A1
List and geometry of muscles used in the neck model.

Muscle	Symmetric multi-segments	Average Length (cm)	PCSA (cm^2)	Density (g/cm^3)
Oblique Captias Inferior	1	3.6	1.713	1.328
Oblique Capitas Superior	1	2.0	0.922	2.268
Rectus Capitus Major	1	4.2	0.541	0.974
Rectus Capitas Minor	1	1.3	0.903	2.371
Longus Capitas	4	8.2	0.892	1.167
Longus Colli	8	10	0.941	0.807
Rectus Capitis Anterior	1	1.9	0.080	1.026
Rectus Capitis Lateral	1	1.1	0.783	1.855
Anterior Scalene	4	9.0	0.821	0.538
Middle Scalene	6	9.3	1.841	0.685
Posterior Scalene	3	7.1	0.892	0.868
Sternocleido Mastoid	2	19.5	2.901	0.685
Illiocostalis Cervicis	4	8.7	0.426	1.053
Longissimus Capitis	5	10.2	0.750	0.719
Longissimus Cervicis	5	9.5	1.586	0.763
Multifidus	6	3.0	4.426	1.290
Semisplenius Capitus	9	15.0	4.267	0.707
Semisplenius Cervicis	4	9.1	3.683	0.596
Splenius Capitis	4	15.5	2.500	0.698
Splenius Cervicis	3	14.0	0.990	0.769
Levator Scapula	4	12.3	2.443	1.026
Minor Rhomboid	2	6.4	0.956	1.493
Trapezius	9	15.8	8.487	0.549
Infrahyoid [a]	3	10.1	2.178	0.714
Suprahyoid [b]	2	3.5	3.170	1.234

[a] The infrahyoid muscle group comprised omohyoid inferior, omohyoid superior, sternothyroid, and thyrohyoid muscles.
[b] The suprahyoid muscle group comprised digastric, geniohyoid, mylohyoid and stylohyoid.

Table A2
Biofidelity rating using the CORA correlation analysis.

Load - muscle	Sub-load	Corridor method	Cross-correlation method				Total score
		Corridor score	*Shape score*	*Size score*	*Phase score*	Cross correlation score	
18g frontal - passive	X-acceleration	0.511	0.896	0.924	0.913	0.907	0.709
	Z-acceleration	0.591	0.910	0.561	1.0	0.845	0.718
	Y- rotational velocity	0.757	0.955	0.827	1.0	0.934	0.845
	Y-moment	0.521	0.896	0.946	1.0	0.934	0.727
	Weighted total						0.750
15g frontal - passive	X-acceleration	0.618	0.0002	0.354	1.0	0.339	0.542
	Z-acceleration	0.148	0.689	0.036	1.0	0.603	0.376
	Y- rotational acceleration	0.04	0.992	0.352	1.0	0.834	0.437
	Weighted total						0.430
15g frontal - active	X-acceleration	0.650	0.997	0.142	1.0	0.784	0.717
	Z-acceleration	0.149	0.684	0.064	1.0	0.608	0.378
	Y- rotational acceleration	0.204	0.908	0.743	1.0	0.890	0.547
	Weighted total						0.547

References

[1] B.S. Myers, B.A. Winkelstein, Epidemiology, classification, mechanism and tolerance of human cervical spine injury, Crit. Rev. Biomed. Eng. 23 (1995) 307–409.

[2] J. Sun, A. Rojas, P. Bertrand, Y. Petit, R. Kraenzler, P.J. Arnoux, Investigation of motorcyclist cervical spine trauma using humos model, Traffic Inj. Prev. 13 (2012) 519–528.

[3] M. Nasim, A. Cernicchi, U. Galvanetto, Development of a finite element neck model for head-first compressive impacts: toward the assessment of motorcycle neck protective equipment, Proc. Inst. Mech. Eng. H: J. Eng. Med. 235 (2021) 1001–1013.

[4] S. Robin, Human model for safety - a joint effort towards the development of refined human-like car occupant models, in: *17th International Technical Conference on Enhanced Safety of Vehicles*, Amsterdam, the Netherlands, 2001, 4–7 JunePaper no. 297.

[5] M.J. van der Horst, PhD Thesis, Eindhoven University of Technology, The Netherlands, 2002.

[6] M. Iwamoto, Y. Kisanuki, I. Wantanabe, K. Furusu, K. Miki, J. Hasegawa, Development of a finite element model of the Total Human Model for Safety (THUMS) and application to injury reconstruction, in: *Conference of IRCOBI*, Munich, Germany, 2002, pp. 31–42.

[7] V.C. Chancey, R.W. Nightingale, C.A. Van Ee, K.E. Knaub, B.S. Myers, Improved estimation of human neck tensile tolerance: reducing the range of reported tolerance using anthropometrically correct muscles and optimizing physiologic initial conditions, Stapp Car Crash J. 47 (2003) 135–154.

[8] K. Brolin, P. Halldin, I. Leijonhufvud, The effect of muscle activation on neck response, Traffic Inj. Prev. 6 (2005) 67–76.

[9] M.B. Panzer, J.B. Fice, D.S. Cronin, Cervical spine response in frontal crash, Med. Eng. Phys. 33 (2011) 1147–1159.

[10] F.S. Gayzik, D.P. Moreno, N.A. Vavalle, A.C. Rhyne, J.D. Stitzel, Development of the global human body models consortium mid-sized male full body model, in: *39th International Workshop on Human Subjects for Biomechanical Research*, NHTS Administration, US DOT, 2011.

[11] J. Östh, M. Mendoza-Vazquez, F. Sato, A. Linder, A female head–neck model for rear impact simulations, J. Biomech. 51 (2017) 49–56.

[12] J.B. Barker, D.S. Cronin, Multilevel validation of a male neck finite element model with active musculature, ASME J. Biomech. Eng. 143 (2021), 011004.

[13] RW Nightingale, J Sganga, H Cutcliffe, C.R.D. Bass, Impact responses of the cervical spine: A computational study of the effects of muscle activity, torso constraint, and pre-flexion, J. Biomech. 49 (2016) 558–564.

[14] H. Gray, Anatomy of the human body, Lea & Febiger, Philadelphia, 2000. - 1918Bartleby.com.

[15] K.L. Moore, A.F. Dalley, Clinically oriented anatomy, 5th ed., Lippincott Williams and Wilkins, Philadelphia, 2006.

[16] J. Borst, P.A. Forbes, R. Happee, H.E.J. Veeger, Muscle parameters for musculoskeletal modelling of the human neck, Clin. Biomech. 26 (2011) 343–351.

[17] W.G. Pearson, S.E. Langmore, A.C. Zumwalt, Evaluating the Structural Properties of Suprahyoid Muscles and their Potential for Moving the Hyoid, Dysphagia 26 (2011) 345–351.

[18] J.O. Hallquist, LS-DYNA keyword user's manual (Volume 2 Version R8.0), Livermore Software Technology Corporation, Livermore, CA, 2015.

[19] J.M. Winters, S.L.Y. Woo, Multiple muscle systems: Biomechanics and movement organization, Springer-Verlag, New York, 1990.

[20] M.F. Griffin, B.C. Leung, Y. Premakumar, M. Szarko, P.E. Butler, Comparison of the mechanical properties of different skin sites for auricular and nasal reconstruction, J Otolaryngol - Head Neck Surg 46 (2017) 33.

[21] J.F.M. Manscho, A.J.M. Brakkee, The measurement and modelling of the mechanical properties of human skin in vivo – II. The model, J. Biomech. 19 (1986) 517–521.

[22] K. Engelbrektsson, MSc. Thesis, Chalmers University of Technology, Gothenburg, 2011.

[23] J.M. Winters, L. Stark, Estimated mechanical properties of synergistic muscles involved in movements of a variety of human joints, J. Biomech. 21 (1988) 1027–1041.

[24] F.E. Zajac, Muscle and tendon: properties, models, scaling, and application to biomechanics and motor control, Crit. Rev. Biomed. Eng. 17 (1989) 359–411.

[25] J.M. Winters, How detailed should muscle models be to understand multi-joint movement coordination? Hum. Movement Sci. 14 (1995) 401–442.

[26] F.A. Pintar, N. Yoganandan, D.J. Maiman, Lower Cervical Spine Loading in Frontal Sled Tests Using Inverse Dynamics: Potential Applications for Lower Neck Injury Criteria, Stapp Car Crash J. 54 (2010) 133–166.

[27] M.W.J. Arun, P. Hadagali, F. Pintar, N. Yoganandan, Normalized frontal impact biofidelity kinematic corridors using post mortem human surrogates, J. Mech. Behav. Biomed. Mater. 79 (2018) 20–29.

[28] C.L. Ewing, D.J. Thomas, G.W. Beeler, L.M. Patrick, D.B. Gillis, Dynamic Response of the Head and Neck of the Living Human to –Gx Impact Acceleration, in: 12th Stapp Car Crash Conference, 1968, pp. 424–439. SAE 680792.

[29] J. Wismans, H. van Oorashot, HJ. Woltring, Omni-directional human head-neck response, in: 30th Stapp Car Crash Conference, 1986, pp. 313–331. SAE 861893.

[30] C.L. Ewing, D.J. Thomas, L. Lustik, G.C. Willems, W.H. Muzzy III, G.W. Beeler, M. E. Jessop, Dynamic response of human and primate head and neck to +Gy impact acceleration, Naval Aerospace Medical Research Laboratory, Pensacola, 1978. Report DOT HS-803-058.

[31] JGM Thunnissen, JSHM Wismans, CL Ewing, et al., Human volunteer head-neck response in frontal flexion: a new analysis, in: 39th Stapp Car Crash Conference, Society of Automotive Engineers, 1995, pp. 439–460. SAE Paper No. 952721.

[32] R.W. Nightingale, J.H. McElhanej, W.J. Richardson, T.M. Best, B.S. Myers, Experimental cervical spine injury: relating head motion, injury classification and injury mechanism, J. Bone Joint Surg. 78 (1996) 412–421.

[33] R.W. Nightingale, J.H. McElhaney, D.L. Camacho, M. Kleinberger, B. A. Winkelstein, B.S. Myers, The dynamic responses of the cervical spine: buckling, end conditions, and tolerance in compressive impacts, SAE Trans. 106 (1997) 3968–3988.

[34] D.L. Camacho, R.W. Nightingale, J.J. Robinette, S.K. Vanguri, D.J. Coates, B. S. Myers, Experimental flexibility measurements for the development of a computational head-neck model validated for near-vertex head impact, SAE Trans. 106 (1997) 3989–4002.

[35] M. Richter, D. Otte, U. Lehmann, B. Chinn, E. Schuller, D. Doyle, K. Sturrock, C. Krettek, Head injury mechanisms in helmet-protected motorcyclists: prospective multicenter study, J. Trauma 51 (2001) 949–958.

[36] C. Gehre, H. Gades, P. Wernicke, Objective rating of signals using test and simulation responses, in: *21st International Technical Conference on Enhanced Safety of Vehicles*, Stuttgart, Germany, 2009. June.

[37] C. Thunet, User's manual of the CORA release (Version 3.6), Partnership for Dummy Technology and Biomechanics (PDB), Germany, 2012.

[38] International Organisation for Standardization (ISO), ISO/TR 16250:2013 Road Vehicles—Objective Rating Metrics for Dynamic Systems. Technical Report, ISO: 56015, ISO, Geneva, Switzerland, 2013.

[39] R.W. Nightingale, D.L. Camacho, A.J. Armstrong, J.J. Robinette, B.S. Myers, Inertial properties and loading rates affect buckling modes and injury mechanisms in the cervical spine, J. Biomech. 32 (2000) 191–198.